DOI: 10.1002/ejic.200601139

Mechanisms of H_2, $H_2C{=}CH_2$, and $O{=}CH_2$ Insertion into $Cp_2Zr(\eta^2\text{-}SiMe_2{=}NtBu)(PMe_3)$

Siwei Bi,*[a] Shufen Zhu,[a] and Zhenwei Zhang[a]

Keywords: Zirconium / Silanimines / Insertion / Mechanism

In this paper, the mechanisms for the insertion of H_2, $H_2C{=}CH_2$, and $O{=}CH_2$ into the Zr–Si bond of $Cp_2Zr(\eta^2\text{-}SiMe_2{=}NtBu)(PMe_3)$ (**R**) are theoretically investigated with the aid of density functional theory (DFT) calculations. The structure of the H_2 insertion product **P** is discussed on the basis of our calculations, and its bonding features are rationalized in terms of molecular orbital theory. The regiochemistry for insertion of $O{=}CH_2$ has also been theoretically investigated. It is found that the relative stabilities of the three insertion products of **R** are in the order $\mathbf{P} < \mathbf{P}' < \mathbf{P}''$. For the reactions of **R** with H_2 and $CH_2{=}CH_2$, the rate-determining steps are the insertions of H_2 and $CH_2{=}CH_2$ into the Zr–Si bond of $Cp_2Zr(\eta^2\text{-}SiMe_2{=}NtBu)$ (**Int1**), whereas PMe_3 dissociation is the rate-determining step for the reaction of **R** with $O{=}CH_2$. Only the precursor **Int2**′′, formed by the coordination of $O{=}CH_2$ to the Zr atom, is located; those formed by the coordination of H_2 and $CH_2{=}CH_2$ to **Int1** are not found.

1. Introduction

Free unsaturated silicon substrates are very reactive and usually exhibit unsaturation at the Si atom. However, they can be stabilized by coordination to transition metals. Metal complexes of silicon analogs of common carbon-based ligands such as silylenes and silaolefins were prepared, but remained quite rare despite their unusual reactivity in chemical transformations, their proposed role in metal-catalyzed transformations at silicon, and their potential utility in the selective formation of silicon-based polymers. Transition-metal complexes of unsaturated silicon compounds such as silenes ($R_2Si{=}CR'_2$), disilenes ($R_2Si{=}SiR_2$), and silanimines ($R_2Si{=}NR'$) are important candidates for experimental and theoretical investigation. The reactions of these complexes with a range of organic and inorganic reagents afford interesting products and provide further insight into the role of such species in catalytic reactions. Remarkable progress has been made over more than ten years in the synthesis of stable transition-metal complexes of unsaturated silicon ligands. In 1988, Tilley and co-workers reported the first stable unsaturated silene complex, $(C_5Me_5)Ru(PR_3)(H)(\eta^2\text{-}R'_2Si{=}CH_2)$.[1,2] Stable mononuclear and binuclear complexes of disilenes were subsequently prepared.[3–8] Okazaki and co-workers prepared a three-membered silametallacyclic complex, $Cp^*Fe(CO)\{\kappa^2(Si,P)\text{-}SiMe_2PPh_2\}$ and studied its reactivity toward MeOH.[9] We have theoretically investigated the mechanisms of formation of the ring-opening products of this reaction.[10] Berry introduced the first unsaturated silanimine complex, $Cp_2Zr(\eta^2\text{-}SiMe_2{=}NtBu)(PMe_3)$,[11] and investigated some chemical reactivity experimentally in 1991. As depicted in Scheme 1, $Cp_2Zr(\eta^2\text{-}SiMe_2{=}NtBu)L$ (L = PMe_3, CO) can react with H_2 by α-bond metathesis, and with olefins, alkynes, aldehydes, or ketones[11,12] by unsaturated bond insertion leading to ring expansion. For these reactions, only the structures of the complexes $Cp_2Zr(\eta^2\text{-}SiMe_2{=}NtBu)(PMe_3)$ and $Cp_2Zr(\eta^2\text{-}SiMe_2{=}NtBu)(CO)$ were determined by single-crystal X-ray diffraction analyses.[11,13] For the complex $Cp_2Zr(\eta^2\text{-}SiMe_2{=}NtBu)(CO)$, the origin of π-back-bonding to the carbonyl ligand directly from an orbital on the adjacent silicon atom has been theoretically investigated by ZINDO molecular orbital calculations.[13] To the best of our knowledge, theoretical studies on the reactions of $Cp_2Zr(\eta^2\text{-}SiMe_2{=}NtBu)(PMe_3)$ with H_2, olefins, alkynes, and aldehydes or ketones have been very limited. For example, the reaction of $[Cp_2ZrHCl]_n$ with $LiNtBuSiMe_2H{\cdot}THF$ in benzene yields $Cp_2ZrH(NtBuSiMe_2H)$, whose structure was characterized by single-crystal X-ray diffraction. The same molecular formalism was afforded by H_2 insertion into the Zr–Si bond of $Cp_2Zr(\eta^2\text{-}SiMe_2{=}NtBu)(PMe_3)$; the product of this reaction has not been analyzed by single-crystal X-ray diffraction. Are the two products obtained from these two reactions the same or different? What structural and bonding features are involved in the product obtained by H_2 insertion? For the reaction of $Cp_2Zr(\eta^2\text{-}SiMe_2{=}NtBu)(PMe_3)$ with $CH_2{=}O$, chemoselectivity clearly appears. Why does the O atom, and not the C atom, of $CH_2{=}O$ bind to the Zr center? In addition, it is necessary to study the reactions in

[a] College of Chemistry Science, Qufu Normal University, Qufu, Shandong, 273165, P. R. China
Fax: +86-537-4456305
E-mail: siweibi@126.com

more detail in order to gain an insight into the mechanisms on these reactions. In this work, theoretical calculations based on the B3LYP DFT have been carried out to examine the structural, bonding, and energetic aspects related to these reaction pathways.

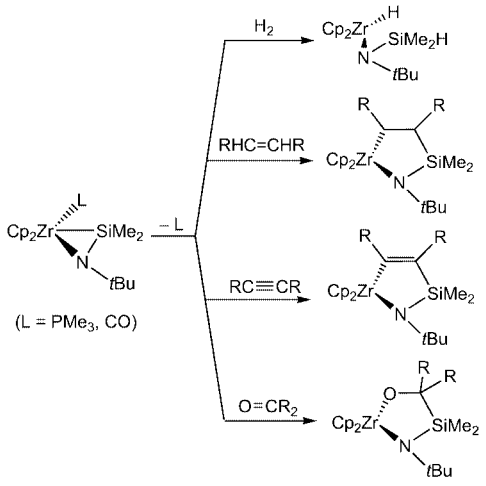

Scheme 1.

As known, the bonding of the silanimine fragment to the metal falls between two resonance extremes. One is a metallacycle in which Si has sp^3 hybridization (X_2 type), and the other is a π-donor complex in which Si has sp^2 hybridization (L type) as shown in the diagram. We will give further evidence for the bonding of the silanimine fragment to the metal on the basis of the results of our calculations.

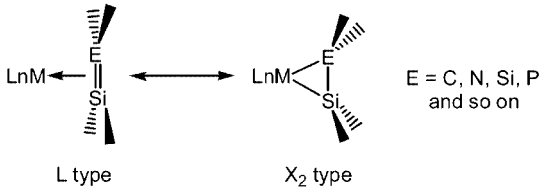

2. Computational Details

All molecular geometries were optimized at the Becke-3LYP (B3LYP) level of DFT.[14–16] Frequency calculations at the same level of theory have also been performed to identify all stationary points as minima (zero imaginary frequencies) or transition states (one imaginary frequency). The transition states involved were checked by IRC (Intrinsic Reaction Coordinate) analysis.[17,18] The effective core potentials (ECPS) of Hay and Wadt with double-ζ valence basis sets (LanL2DZ) were used to describe Zr, Si, and P atoms, while the standard 6-31G basis set was used to describe C, N, and H atoms. Polarization functions were added for P(ζ d = 0.34), Si(ζ d = 0.262), N(ζ d = 0.8), and those atoms directly involved in bond-forming and bond-breaking processes, C(ζ d = 0.8), H(ζ p = 0.11). All the calculations were performed with the Gaussian 98 software package.[19]

For examining the feasibility of the B3LYP level of DFT, the computed geometrical structure of the reactant **R** was compared to the original X-ray diffraction structure. Selected calculated and experimental (in brackets) bond lengths are shown in Figure 2. The calculated values and the geometrical parameters obtained from X-ray diffraction are close enough, indicating that our calculations at the B3LYP level of DFT are reliable. We have also used this computational method to investigate other organometallic systems.[20–23]

3. Results and Discussion

For investigating the mechanisms, the structures, and the bonding features involved in the reactions mentioned above, we chose H_2, $H_2C{=}CH_2$, and $O{=}CH_2$ as substrates to react with $Cp_2Zr(\eta^2\text{-}SiMe_2{=}N\mathit{t}Bu)(PMe_3)$ (**R**). The mechanisms for the three reactions are theoretically proposed as shown in Scheme 2. Since the reactant **R** is coordinatively saturated, it is proposed that **R** first loses the phosphane ligand, PMe_3, through a transition state **TS1**, to form a 16-electron intermediate **Int1**. In reaction (1), **Int1** reacts with H_2 to yield the product **P** via a transition state **TS2**. In reaction (2), **Int1** reacts with ethylene to give the product **P′** via a transition state **TS2′**. In reaction (3), **Int1** reacts with formaldehyde to afford the product **P′′** via a transition state **TS2′′**.

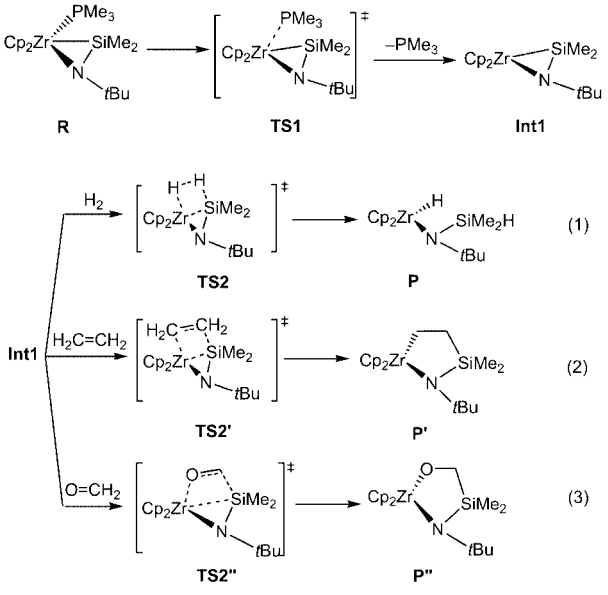

Scheme 2.

3.1 Insertion of H_2

Figure 1a shows the calculated potential energy profile corresponding to the reaction of **R** with H_2 by the mechanism shown in Scheme 2. Figure 2 shows all the B3LYP-optimized geometrical structures with selected structural parameters. The first step is the dissociation of PMe_3. In **R**

and **TS1**, the calculated Zr–P bond lengths are 2.76 and 3.73 Å, respectively, indicating that the PMe_3 leaves from the metal center. Table 1 indicates that the Zr–Si and Zr–N bond lengths decrease and the Si–N bond length increases in going from **R** via **TS1** to **Int1**. This means that, with the dissociation of PMe_3, the $Me_2SiNtBu$ unit tends to be closer to the Zr center, and correspondingly the interaction between the $Me_2SiNtBu$ unit and Zr is enhanced. The Si–N bond is then weakened with the increasing interaction of the Zr center with the $Me_2SiNtBu$ unit, and hence the Si–N bond length increases in going from **R** via **TS1** to **Int1**, as shown in Table 1. Also, as the $Me_2SiNtBu$ unit approaches the Zr atom, the increasing strain in the Zr–Si–N ring in going from **R** to **Int1** can make the Si–N bond longer. Clearly, this structural variation results from the loss of the PMe_3 ligand. The activation energy for the step from **R** to **Int1** is calculated to be 9.2 kcal/mol. **Int1** is higher than **R** in energy by 5.9 kcal/mol, indicating that this step is thermodynamically unfavorable. The reason for the instability of **Int1** compared with **R** is the transformation from the 18-electron species **R** to the 16-electron species **Int1**.

Table 1. Zr–N, Zr–Si, and Si–N bond lengths [Å] in all the species involved in the reaction mechanism shown in Figure 1a.

	Zr–N	Zr–Si	Si–N
R	2.16	2.67	1.72
TS1	2.09	2.62	1.76
Int1	2.07	2.60	1.77
TS2	2.09	2.62	1.75
P	2.20	2.94	1.71

As for step two (**Int1** to **P**), the results of our calculations indicate that insertion of H_2 into the Zr–Si bond becomes energetically accessible as shown in Figure 1a. The H–H bond length in free H_2 is calculated to be 0.74 Å. In **TS2**, the calculated H1–H2, Zr–Si, Zr–H1, and Si–H2 bond lengths are 0.76, 2.62, 2.72, and 2.89 Å, respectively. As H_2 approaches the metal center in **TS2**, the H1–H2 and Zr–Si bonds are elongated with respect to their values in **Int1**. The activation energy for the step is calculated to be 7.8 kcal/mol. In the product **P**, the H1–H2 and Zr–Si bonds are broken, and Zr–H1 and Si–H2 σ bonds are formed. As shown in Table 1, the Zr–Si bond length increases in going from **Int1** via **TS2** to **P** as a result of the insertion of H_2. The Si–N bond strength is enhanced as a result of the decrease in the π-back-donation from the metal center to the Si–N unit and the release of the ring strain. As indicated in Table 1, the Si–N bond length decreases in going from **Int1** via **TS2** to **P**. The Zr–N bond length increases slightly as shown in Table 1, which arises mainly from two factors. One is the decrease in the π-back-donation, which weakens the Zr–N bond. The other is the increasing steric hindrance of the *t*Bu group attached to the N atom by the two Cp rings because of the increase in the Zr–N–Si bond angle. The energy difference for the step is calculated to be –17.7 kcal/mol, indicating that this step is very much favored thermodynamically.

Examining carefully the structure of **P**, we predict the presence of an agostic interaction between the Si–H bond and the metal center. Evidence offered by our calculations is as follows: (i) The Zr, N, Si, and C1 atoms are coplanar, and hence the N atom has sp^2 hybridization. Thus, the Zr–N–Si bond angle could be predicted to be about 120°. However, this angle is calculated to be 96.4°, supporting the occurrence of an interaction between the Zr atom and the Si–H bond. (ii) The Si atom has sp^3 hybridization, and hence the N–Si–H2 bond angle could be predicted to be about 109°. In fact, the bond angle is calculated to be 95.2°, also providing evidence for the agostic interaction. (iii) The Si–H2 bond length is calculated to be 1.54 Å. This bond could be expected to be longer in the absence of an agostic interaction. For investigating the Si–H2 bond length, we designed a model complex, **A**, as shown in Figure 2. **A** is derived from the product **P** by the replacement of the two methyl groups attached to the Si atom by two hydrogen atoms. The Si–H3 and Si–H4 bond lengths in **A** are calculated to be 1.49 Å, and the Si–H2 bond length in **A** is 1.52 Å. Clearly, the Si–H2 bond is longer than both the Si–H3 and the Si–H4 bonds, implying the presence of an agostic interaction between the Si–H2 bond and the Zr atom in **A**, and further supporting the prediction of an agostic interaction in **P**. Even though Zr has d^0 configuration, meaning that little back-donation from Zr to the σ* orbital of Si–H is present, the agostic interaction is still present. The greater stability of **P** compared with **Int1** has two main reasons. One is the release of the strain in the Zr–N–Si three-membered ring. The other is the presence of the agostic interaction mentioned above. The agostic interaction helps the complex achieve a formal 18-electron configuration, and hence makes some contribution to the stability of **P**. To the best of our knowledge, the structure of **P** has not been characterized by single-crystal X-ray diffraction. However, the structure of an isomer of **P**, represented by **P**-isomer in this paper, was analyzed by single-crystal X-ray diffraction.[24] **P**-isomer was prepared from the reaction of $[Cp_2ZrHCl]_n$ with $LiNtBuSiMe_2H{\cdot}THF$ in benzene as shown in Scheme 3. The structure of **P**-isomer is optimized at the same level of B3LYP, which is illustrated in Figure 2 with selected bond lengths. The calculated Zr–N and N–Si bond lengths (2.17, 1.72 Å, respectively) are close to the experimental observations (2.14, 1.71 Å). The results of our calculations are consistent with the experimental analysis results that an agostic interaction between Zr and the Si–H bond is present in the compound. The Zr···H1 distance and the N–Si–H1 angle in **P**-isomer are calculated to be 2.29 Å and 95.7°, respectively; these values are similar to those in **P** (2.20 Å, 95.2°). The calculated Zr–N–Si bond angle is 98.8°, which is close to that in **P** (96.4°) and to the experimental result (95.1°).[24] On the basis of the structural parameters above, we can also theoretically support the presence of the β-agostic interaction mentioned above. **P**-isomer is calculated to be more stable than **P** by –2.0 kcal/mol. The weaker steric hindrance in **P**-isomer compared with that in **P** may be responsible for its relative stability. Theoretically, **P** could be converted into the more stable **P**-isomer by rota-

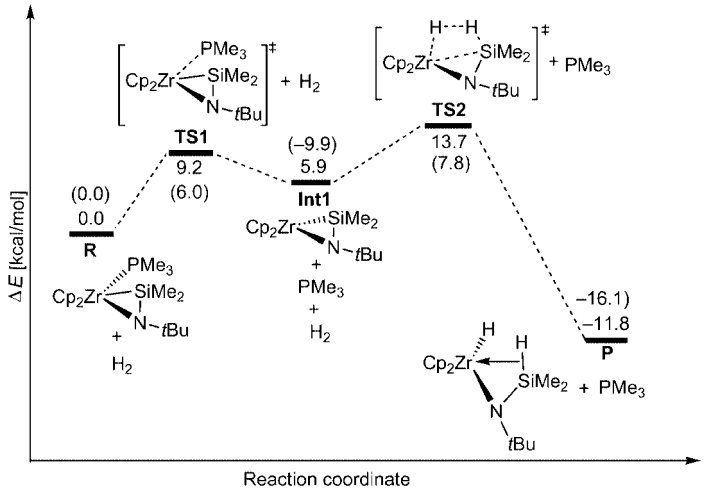

(a)

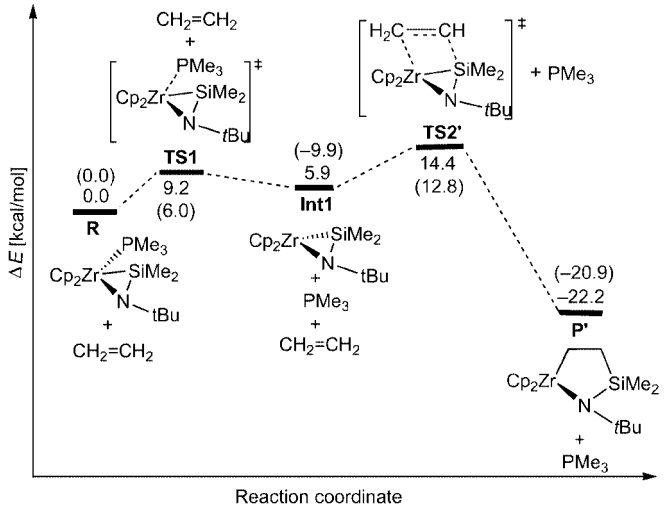

(b)

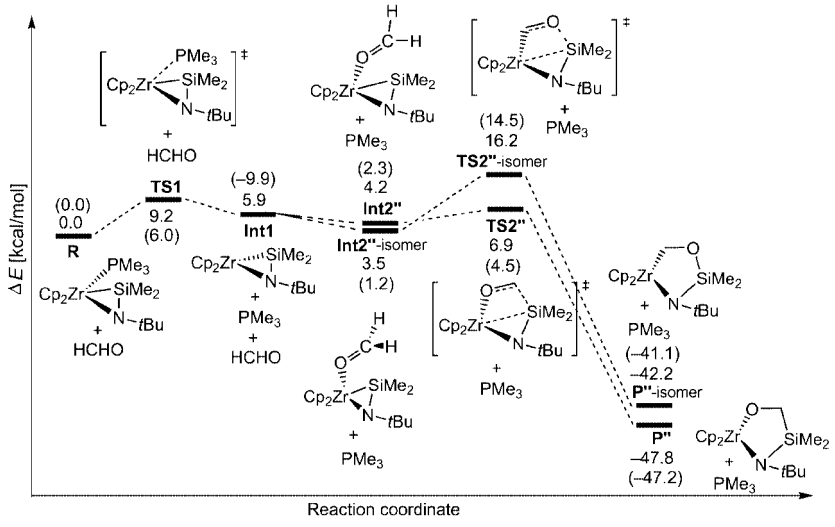

(c)

Figure 1. (a) Energy profile for the insertion reaction of H_2 into $Cp_2Zr(\eta^2\text{-}SiMe_2{=}NtBu)(PMe_3)$. (b) Energy profile for the insertion reaction of ethylene into $Cp_2Zr(\eta^2\text{-}SiMe_2{=}NtBu)(PMe_3)$. (c) Energy profile for the insertion reaction of formaldehyde into $Cp_2Zr(\eta^2\text{-}SiMe_2{=}NtBu)(PMe_3)$. The relative energies and free energies (in parentheses) are given in kcal/mol.

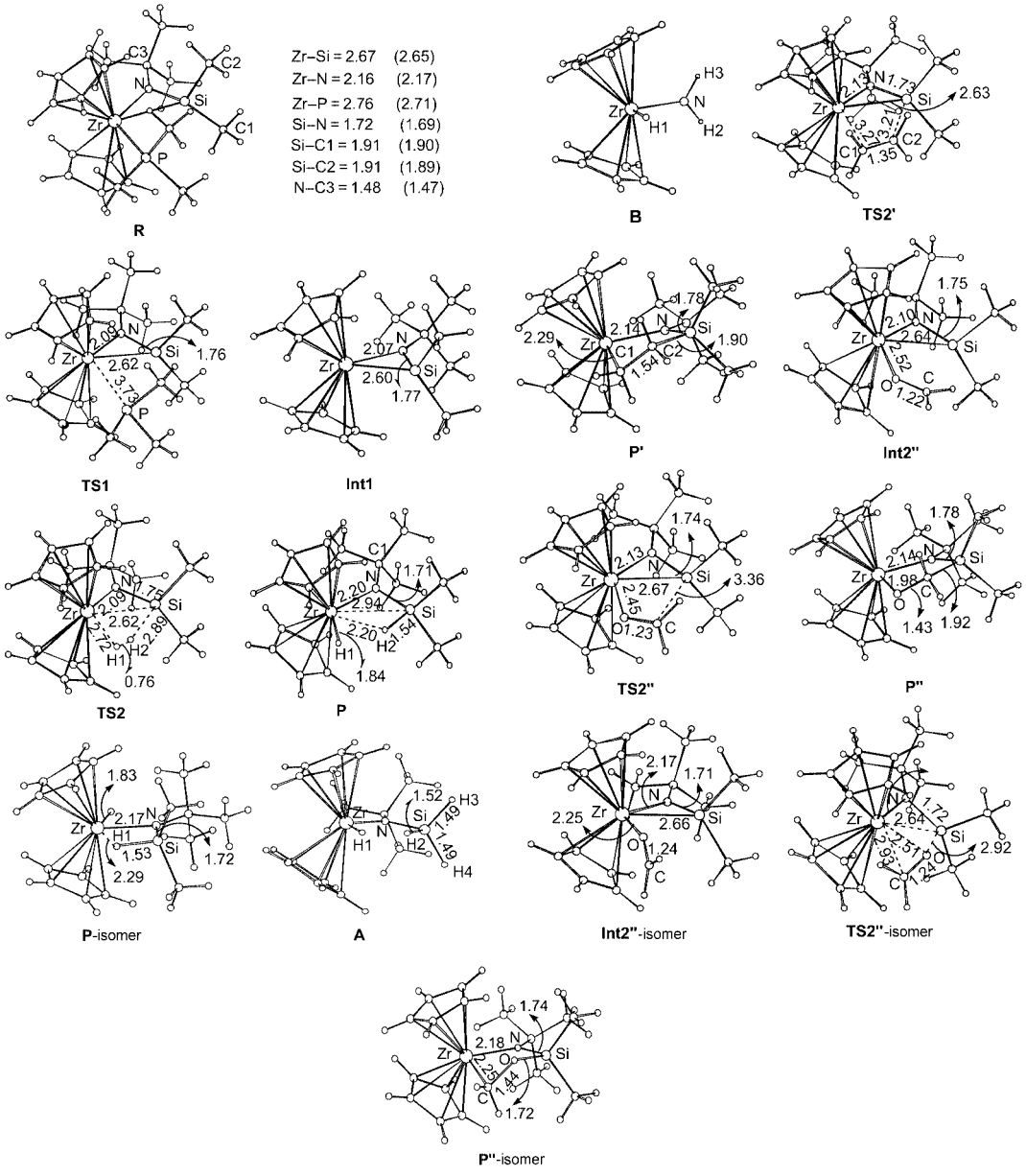

Figure 2. B3LYP-optimized structures of all related compounds with selected structural parameters. The experimental data are given in brackets. Bond lengths are in Å.

tion of –N(*t*Bu)($SiMe_2H$) about the Zr–N axis. However, the conversion through rotation is very difficult because of the agostic interaction and the steric hindrance as mentioned above. So, we suggest theoretically that the final product for reaction (1) in Scheme 2 is **P** but not **P**-isomer.

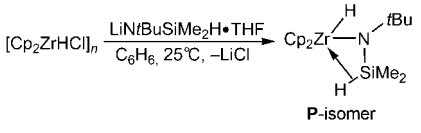

Scheme 3.

It is interesting to further discuss the structure of the product **P** and the bonding features involved. If the *t*Bu and $SiHMe_2$ groups are substituted by two hydrogen atoms, the B3LYP-optimized structure of the derived model complex, $Cp_2ZrH(NH_2)$ (**B**), shown in Figure 2, is different from that of **P**. The Zr, N, H2, and H3 atoms are coplanar, meaning that the N atom has sp^2 hybridization, and one lone pair is on the p orbital of the N atom perpendicular to the Zr–N–H2–H3 plane. The H1–Zr–N–H2 and H1–Zr–N–H3 dihedral angles are calculated to be equal (89.4°). In other words, the H2–N–H3 plane is perpendicular to the H1–Zr–N plane in **B**, whereas H1, Zr, N, C1, and Si are coplanar in **P**. The structural difference between **P** and **B** is worth to explore in terms of molecular orbital interactions. For the model complex $Cp_2ZrH(NH_2)$, only if the H2–N–H3 plane is perpendicular to the H1–Zr–N plane can the lone pair on the N atom have the same symmetry with one

LUMO ($1a_1$) of the fragment Cp_2M, as shown in Scheme 4.[25] Thus, the π interaction between $1a_1$ and the p orbital takes effect, and the Zr–N bond is further stabilized. Therefore, the π interaction between the $1a_1$ orbital of the fragment Cp_2M and the p orbital on the N atom is responsible for the orientation of the H2–N–H3 plane. In contrast, the C1–N–Si plane in **P** is wedged into the two Cp rings. Clearly, the π interaction mentioned above is not present in **P**, since the LUMO ($1a_1$) is not symmetric to the p orbital on the N atom. Other factors play a dominant role in controlling the geometrical structure. One is the agostic interaction between Zr and the Si–H bond, which prevents the rotation of the C1–N–Si plane around the Zr–N axis. Another is the steric hindrance of the two Cp rings, affecting the bulky *t*Bu and $SiHMe_2$ groups, which also blocks the rotation of the C1–N–Si plane around the Zr–N axis. Only when the C1–N–Si plane is wedged into the two Cp rings can the steric effect be reduced to the least possible amount.

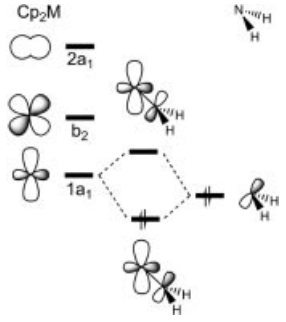

Scheme 4.

Figure 1a shows that the rate-determining step is the insertion of H_2 into the Zr–Si bond. The reaction activation energy is calculated to be 13.7 kcal/mol. The product **P** is lower in energy than the reactant **R** by 11.8 kcal/mol, indicating that the reaction is thermodynamically favorable. The high stability of the product **P** relative to the reactant **R** arises mainly from the release of the strong ring strain in going from **R** to **P**, the formation of the relatively strong Zr–H bond, and the agostic interaction of the Si–H bond with the metal center.

The bonding between Zr and the Si–N is also worth discussing. As mentioned in the introduction, there are two extremes for the structure of the Zr–Si–N three-membered ring, the L type and the X_2 type. What we want to know is which one is the major type in the reactant **R**. First, we take a look at the structure of the product **P**. The Si atom in **P** has sp^3 hybridization, and hence the Si–N bond is a σ bond. The bond length is calculated to be 1.71 Å. In the reactant **R**, both N and Si atoms bind to the metal, and the Si–N bond length is calculated to be 1.72 Å, which is even slightly longer than that in **P**, suggesting that the Zr–Si–N unit has X_2-type bonding. This is a result of the fact that the remaining d^2 electrons in the fragment Cp_2Zr are very reactive, and hence the Cp_2Zr fragment is a very good π base. The two methyl groups attached to the Si atom are bent far away from the metal, which is also consistent with the X_2-type structure. The Zr–N bond in **P** is a σ bond, which is longer than that in **R** only by 0.04 Å, also suggesting that the Zr–N bond in **R** is a σ bond.

3.2 Insertion of $CH_2{=}CH_2$

Reaction (2) in Scheme 2 is the insertion of ethene into the Zr–Si bond. Figure 1b shows the energy profile corresponding to the reaction mechanism. Related geometrical structures with selected structural parameters are also illustrated in Figure 2. The first step is the same as that in reaction (1). The second step is the insertion of the C=C double bond into the Zr–Si bond. In **TS2′**, the calculated Zr···C1 and Si···C2 distances are 3.27 and 3.21 Å, respectively. The Zr–Si bond length is 2.63 Å, which is slightly larger than that in **Int1** (2.60 Å). The C1–C2 bond length (1.35 Å) is almost the same as the free ethylene C–C bond length, indicating that the C1 and C2 atoms keep nearly sp^2 hybridization. Clearly, **TS2′** is a very early transition state. IRC analysis confirms that **TS2′** directly connects to **Int1** and the product **P′**. In other words, along the reaction coordinate, no precursor in which ethylene is coordinated to the metal center can be located as a minimum on the potential energy profile. The reason is probably that the d^0 metal center cannot stabilize an olefin complex because of lack of back-donation. The activation energy for the step is calculated to be 8.5 kcal/mol. When the ethylene ligand is inserted into the Zr–Si bond, a five-membered metallacycle is formed in the product **P′**. The hybridizations of C1 and C2 are changed from sp^2 to sp^3, which is supported by change in the C1–C2 bond length from 1.35 Å in **TS2′** to 1.54 Å in **P′**. No agostic interaction between C–H and Zr is found because of the formation of the metallacycle. The energy difference for the step is calculated to be –28.1 kcal/mol, indicating that this step is thermodynamically very favorable . The high stability of **P′** relative to **Int1** is a result of the chelating effect involved and the releasing of ring strain.

As shown in Figure 1b, the rate-determining step is the insertion of ethylene into the Zr–Si bond. The reaction activation energy is calculated to be 14.4 kcal/mol, which is slightly higher than that for H_2 insertion. The reaction energy difference is –22.2 kcal/mol. Although the reactant **R** is an 18-electron species, **R** is much less stable than the 16-electron product **P′**. The reasons for the energy difference are the releasing of ring strain from **R** to **P′** and the chelating effect involved in **P′**.

3.3 Insertion of $CH_2{=}O$

Figure 1c shows the energy profile for the reaction of **R** with the substrate formaldehyde. Related B3LYP geometrical structures are illustrated in Figure 2. In contrast to the insertion of H_2 and ethylene, a precursor, **Int2′′**, is located for the insertion of formaldehyde. In the structure of **Int2′′** shown in Figure 2, the Zr–O bond length is calculated to be 2.52 Å. The C–O bond length in the coordinated CH_2O is 1.22 Å, while that in free CH_2O is 1.21 Å, calculated at

the same level of theory, which supports the coordination of CH_2O to the metal center. The calculated distance between the Zr atom and the C atom of CH_2=O is 3.44 Å, indicating that the O atom is coordinated to the metal center rather than the CH_2=O π bond. This means that the binding of the terminal oxygen coordination is stronger than that of the side C=O coordination. The reason for the different binding ability is that the metal center Zr^{IV} is a hard acid and the O atom is a hard base, which can form a relatively strong σ coordination bond to afford an 18-electron intermediate. **Int2′′** is more stable than **Int1** by 1.7 kcal/mol. The coordination of CH_2O to the metal to achieve an 18-electron species may be responsible for the relatively high stability of **Int2′′** relative to **Int1**. The coordination abilities of the substrates studied in this paper to the Zr center are in the order PMe_3 > CH_2O > CH_2=CH_2 > H_2. The calculated results show that **R** is more stable than **Int2′′**, whereas the precursors formed by the coordination of ethylene and dihydrogen to the Zr atom are not present.

Ring expansion from **Int2′′** to **P′′** results from the insertion of the C=O bond of CH_2=O into the Zr–Si bond. Obviously, the regiochemistry of the C=O insertion could occur in two modes: one would be the binding of the Zr with the O atom and Si with the C atom, and the other would be the binding of the Zr with the C atom and Si with the O atom. Experiments confirmed that the O atom is coordinated to the Zr atom to afford a five-membered metallacycle in **P′′**. This results from the fact that the Zr^{IV} is a hard acid and the O atom is a hard base in terms of the so-called "hard soft acid base theory", leading to the relatively strong interaction between the Zr and O atoms.

In the calculated insertion transition state **TS2′′**, the calculated Zr–O bond length is 2.45 Å, and the Si···C distance is 3.36 Å. IRC calculations confirmed that **TS2′′** directly connects to **Int2′′** and **P′′**. The longer Zr–N and Zr–Si bond lengths than those in **Int2′′** indicate a decrease in π-back-donation from the metal to the Si–N unit. Consequently, the Si–N bond becomes slightly shorter than that in **Int2′′**. The C–O bond length in **TS2′′** is calculated to be 1.23 Å, which is larger than that in **Int2′′**. The longer Zr–Si and C–O bonds and shorter Zr–O and Si–C bonds imply stronger interaction between the latter two bonds relative to that in **Int2′′**. In the structure of **P′′**, a five-membered ring containing the metal center is formed. The Si atom is far away from the metal center, and the three σ bonds (Zr–O, O–C, and C–Si) are formed; this can be confirmed by the structural parameters of **P′′** shown in Figure 2. The activation energy for the step is calculated to be 2.7 kcal/mol, indicating the insertion of formaldehyde is kinetically much favorable. The energy difference for the step is calculated to be –52.0 kcal/mol. In contrast to the insertion of H_2 and ethylene, the rate-determining step of Reaction (3) in Scheme 2 is theoretically predicted to be the dissociation of the phosphane ligand PMe_3 and not the insertion of C=O into the Zr–Si bond. The strong interaction between the Zr and O atoms plays a crucial role in stabilizing the transition state **TS2′′**. The reaction energy is calculated to be –47.8 kcal/mol, indicating that this reaction is much favorable thermodynamically. Releasing of ring strain and the chelating effect due to the formation of the five-membered metallacycle are responsible for the favored thermodynamics.

Clearly, there is regioselectivity in the insertion of O=CH_2. The metal could be attacked by the O atom of O=CH_2 or by the C atom. As shown in Figure 1c, the transition state **TS2′′**-isomer is located, which connects an intermediate **Int2′′**-isomer and a proposed product **P′′**-isomer. In this step, the C atom is bound to Zr and the O atom bound to Si. Calculations show that **Int2′′**-isomer is more stable than **Int2′′** by 0.7 kcal/mol. This arises from the stronger Zr–O bond in **Int2′′**-isomer than that in **Int2′′**, since the Zr–O bond length is shorter in the former (2.25 Å) than in the latter (2.52 Å). The **TS2′′**-isomer is calculated to be higher in energy than **TS2′′** by 9.3 kcal/mol. The reason for this energy difference can be understood by an energy-decomposition analysis of reaction barriers.[26,27] As shown in Scheme 5, ΔE_1 and ΔE_2 represent the binding energies between **TS2′′**-frag and **TS2′′**, and **TS2′′**-isomer-frag and **TS2′′**-isomer, respectively. ΔE_3 is the energy difference between the two kinds of fragments. ΔE_4 is the activation energy difference between **TS2′′** and **TS2′′**-isomer. It can be seen in Scheme 5 that $\Delta E_4 = (\Delta E_1 - \Delta E_2) - \Delta E_3$ = –5.9–3.5 = –9.4 (kcal/mol). The binding energy difference (–5.9 kcal/mol) plays a dominant role in the difference between the activation energies. Clearly, the stronger Zr–O bond in **TS2′′** relative to the Zr–C bond in **TS2′′**-isomer is responsible for the activation energy difference. The isomer of **P′′**, **P′′**-isomer, is 5.6 kcal/mol higher in energy than **P′′**. The driving force from **Int2′′** to **P′′**, but not to **P′′**-isomer is still the strong interaction of the O atom with the metal center.

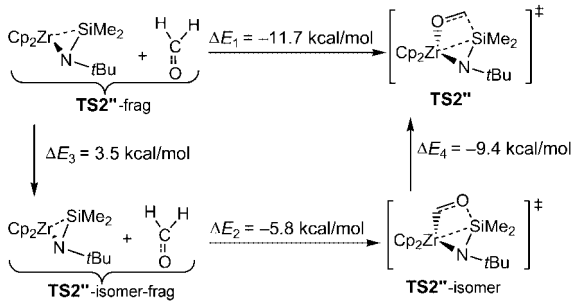

Scheme 5.

3.4 Comparison of the Insertions of H_2, CH_2=CH_2, and CH_2=O

In a comparison of the three reactions, insertion of H_2 can be regarded as a σ-bond metathesis, while insertion of ethylene and formaldehyde are processes of ring expansion. The reactant **R** is an 18-electron species, so we propose that the first step is the dissociation of PMe_3 to give a 16-electron intermediate. Among the insertions of the three substrates, only that of formaldehyde involves a precursor formed by the coordination of formaldehyde to the Zr cen-

ter as a result of the strong interaction between the so-called "hard acid" Zr^{IV} center and the so-called "hard base" O atom of CH_2=O. The precursors formed by coordination of H_2 and CH_2=CH_2 are theoretically predicted to be nonexistent, mainly owing to the lack of back-donation, as the Zr center has d^0 configuration. As for the three transition states, **TS2**, **TS2′**, and **TS2′′**, the former two are relatively close to each other. H_2 has a higher bond energy than the ethylene π bond, indicating that the H–H σ bond is more difficult to break than the C=C π bond. However, ethylene engages in a larger steric repulsive interaction as it approaches the metal center, while H_2 can easily reach the metal center with its much less bulky structure. These two factors lead to similar activation energies for the two insertions. In comparison, the transition state **TS2′′** for the insertion of formaldehyde is much lower than **TS2** and **TS2′** in energy, and even lower than the dissociation barrier of PMe_3, as a result of the strong interaction between the Zr and O atoms. Therefore, in contrast to the insertion of H_2 and ethylene, the rate-determining step for reaction (3) in Scheme 2 becomes the dissociation of PMe_3 and not the insertion of formaldehyde. Figure 1 indicates that the relative stability of the three products with respect to the reactant **R** is in the order **P** < **P′** < **P′′**. A chelating effect due to the formation of the five-membered metallacycle in **P′** and **P′′** leads to the higher stability of **P′** and **P′′** relative to **P**. For early transition metals, M–X (X is a heteroatom) bonds are much stronger than M–C bonds.[28] For example, calculated results show that the bonding energy difference between Ta–OH and Ta–C bonds is about 53.1 kcal/mol, and the difference between Ta–Cl and Ta–C bonds is about 35.6 kcal/mol. For late transition metals, M–X bonds are a little stronger than M–C bonds. For example, the bond dissociation energy of a Pt–Cl bond is estimated to be only about 10.0 kcal/mol larger than that of a Pt–C bond.[29,30] The energy of **P′** is calculated to be –22.2 kcal/mol, while that of **P′′** is –47.8 kcal/mol with respect to the reactant **R**. **P′′** is much more stable than **P′**. Clearly, the reason for the higher stability of **P′′** is the formation of the strong Zr–O σ bond.

4. Conclusions

Metal complexes of silanimines ($R_2Si{=}NR'$) exhibit unusual reactivity in chemical transformations. The reactions of these complexes with a range of organic and inorganic reagents yield interesting products and provide further insight into the role of such species in catalytic reactions. Three typical insertion reactions, those of H_2, CH_2=CH_2, and CH_2=O into the Zr–Si bond of $Cp_2Zr(\eta^2\text{-}SiMe_2{=}NtBu)(PMe_3)$ were chosen to investigate their reaction mechanisms and the structural and bonding features involved in these reactions. The product of H_2 insertion, **P**, is structurally discussed, and we find that a Zr···H–Si agostic interaction is present. The bonding feature in **P** is analyzed in comparison to the designed model complex $Cp_2Zr(NH_2)H$ (**B**). The geometrical structural difference between **P** and **B** results from their different bonding properties and steric environments. We also predict that the H_2 insertion product, **P**, is different from **P**-isomer, the product obtained from the reaction of $[Cp_2ZrHCl]_n$ with $LiNtBuSiMe_2H{\cdot}THF$. The results of our calculations also confirm that the product of CH_2=O insertion contains the Zr–O bond and not the Zr–C bond as a result of the stronger interaction of Zr with the O atom than with the C atom.

The reaction mechanisms are confirmed theoretically to comprise two steps, dissociation of PMe_3 and insertion of H_2, CH_2=CH_2, and CH_2=O. Theoretical findings are: (i) the relative stabilities of the three insertion products of **R** are in the order **P** < **P′** < **P′′**; (ii) the rate-determining step is H_2 insertion in reaction (1) and CH_2=CH_2 insertion in reaction (2), whereas it is PMe_3 dissociation in reaction (3); (iii) only the precursor **Int2′′** is located, while those formed by the coordination of H_2 and CH_2=CH_2 to **Int1** are not found.

Acknowledgments

This work was supported by the National Science Foundation of China (No.: 20473047).

[1] B. K. Campion, R. Heyn, T. D. Tilley, *J. Am. Chem. Soc.* **1988**, *110*, 7558.
[2] B. K. Campion, R. Heyn, T. D. Tilley, *J. Am. Chem. Soc.* **1990**, *112*, 4079.
[3] E. K. Pham, R. West, *J. Am. Chem. Soc.* **1989**, *111*, 7667–7668.
[4] E. K. Pham, R. West, *Organometallics* **1990**, *9*, 1517.
[5] D. H. Berry, J. H. Chey, H. S. Zipin, P. J. Carroll, *J. Am. Chem. Soc.* **1990**, *112*, 452.
[6] E. A. Zarate, C. A. Tessier-Youngs, W. J. Youngs, *J. Am. Chem. Soc.* **1988**, *110*, 4068–4070.
[7] E. A. Zarate, C. A. Tessier-Youngs, W. J. Youngs, *J. Chem. Soc., Chem. Commun.* **1989**, 577–578.
[8] A. E. Anderson, P. Shiller, E. A. Zarate, C. A. Tessier-Youngs, W. J. Youngs, *Organometallics* **1989**, *8*, 2320.
[9] M. Okazaki, K. A. Jung, H. Tobita, *Organometallics* **2005**, *24*, 659–664.
[10] X. Zhu, B. Zhao, B. Wang, Y. Zhao, S. Bi, *Chem. Phys. Lett.* **2006**, *422*, 6–10.
[11] L. J. Procopio, P. J. Carroll, D. H. Berry, *J. Am. Chem. Soc.* **1991**, *113*, 1870–1872.
[12] L. J. Procopio, P. J. Carroll, D. H. Berry, *Organometallics* **1993**, *12*, 3087–3093.
[13] L. J. Procopio, P. J. Carroll, D. H. Berry, *Polyhedron* **1995**, *14*, 45–55.
[14] C. S. Cramer, *Essentials of Computational Chemistry, Theories and Models*, John Wiley & Sons, New York, **2002**.
[15] C. Lee, W. Yang, G. Parr, *Phys. Rev. B* **1988**, *37*, 785.
[16] A. D. Becke, *J. Chem. Phys.* **1993**, *98*, 5648.
[17] C. Gonzalez, H. B. Schlegel, *J. Chem. Phys.* **1989**, *90*, 2154.
[18] C. Gonzalez, H. B. Schlegel, *J. Chem. Phys.* **1990**, *94*, 5523.
[19] M. J. Frisch, G. W. Trucks, H. B. Schlegel, G. E. Scuseria, M. A. Robb, J. R. Cheeseman, V. G. Zakrzewski, J. A. Montgomery Jr, R. E. Stratmann, J. C. Burant, S. Dapprich, J. M. Millam, A. D. Daniels, K. N. Kudin, M. C. Strain, O. Farkas, J. Tomasi, V. Barone, M. Cossi, R. Cammi, B. Mennucci, C. Pomelli, C. Adamo, S. Clifford, J. Ochterski, G. A. Petersson, P. Y. Ayala, Q. Cui, K. Morokuma, D. K. Malick, A. D. Rabuck, K. Raghavachari, J. B. Foresman, J. Cioslowski, J. V. Otitz, B. B. Stefanov, G. Liu, A. Liashenko, P. Piskorz, I. Komaromi,

R. Gomperts, R. L. Martin, D. J. Fox, T. Keith, M. A. Al-Laham. C. Y. Peng, A. Nanayakkara, C. Gonzales, M. Challacombe, P. M. W. Gill, B. Johnson, W. Chen, M. W. Wong, J. L. Andres, M. Head-Gordon, E. S. Replogle, and J. A. Pople, *Gaussian 98 Revision A.5*, Gaussian, Inc., Pittsburgh, PA, **1998**.
[20] S. Bi, Z. Lin, R. F. Jordan, *Organometallics* **2004**, *23*, 4882–4890.
[21] S. Bi, A. Ariafard, G. Jia, Z. Lin, *Organometallics* **2005**, *24*, 680–686.
[22] S. Bi, B. Wang, Y. Zhao, Z. Zhang, S. Zhu, *Chem. Phys. Lett.* **2006**, *426*, 192–196.
[23] A. Ariafard, S. Bi, Z. Lin, *Organometallics* **2005**, *24*, 2241–2244.
[24] L. J. Procopio, P. J. Carroll, D. H. Berry, *J. Am. Chem. Soc.* **1994**, *116*, 177–185.
[25] T. A. Albright, J. K. Burdett, M.-H. Whangbo, *Orbital Interactions in Chemistry*, John Wiley & Sons, New York, **1985**, pp. 394–398.
[26] T. Ziegler, A. Rauk, *Theor. Chim. Acta* **1977**, *46*, 1.
[27] J. Zhu, G. Jia, Z. Lin, *Organometallics* **2006**, *25*, 1812–1819.
[28] T. R. Cundari, C. D. Taylor, *Organometallics* **2003**, *22*, 4047.
[29] G. Altakhin, H. A. Skinner, A. A. Zaki, *J. Chem. Soc., Dalton Trans.* **1984**, 371.
[30] S. R. Foley, R. A. Stockland, H. Shen, R. F. Jordan, *J. Am. Chem. Soc.* **2003**, *125*, 4350.

Received: December 1, 2006
Published Online: April 10, 2007

